



ZnO nanobridge devices fabricated using carbonized photoresist

B.D. Pelatt*, C.C. Huang, J.F. Conley Jr.

School of Electrical Engineering and Computer Science, Oregon State University, Corvallis, OR 97331, United States

ARTICLE INFO

Article history:

Available online 16 June 2010

The review of this paper was arranged by Prof. A. Zaslavsky

Keywords:

Nanotechnology
Nanowire
ZnO
Integration
Electrical characterization

ABSTRACT

Despite high interest for novel device applications, alignment and electrical integration of nanowires to lithographically defined features remains a challenge. In this work, ZnO nanowire devices were fabricated using a novel carbonized photoresist method in which photoresist is lithographically patterned, carbonized at elevated temperature, and then used to selectively seed growth of ZnO nanobridges between opposing carbonized photoresist electrodes. The pick and place method is avoided and selective growth of nanobridge structures is achieved without the use of metal catalysts or inorganic seed layers. Growth and electrical connection take place simultaneously. Electrical characterization of the electrical contact between the carbonized photoresist electrodes and the ZnO nanobridges is performed and operation of nanobridge devices as bottom gate three terminal field effect devices is demonstrated.

© 2010 Elsevier Ltd. All rights reserved.

1. Introduction

Nanowire (NW) devices have shown great promise for optoelectronic, sensing, and piezoelectric applications [1–5]. However, most devices to date have been demonstrated using harvest and disperse (pick and place) type methods in which NWs are grown on one substrate, harvested into solution using sonication, and then dispersed randomly onto a device substrate. Nanowire devices are then typically constructed individually using e-beam techniques. Large scale integration of NWs (alignment and contact to lithographically defined features) remains a challenge. Although dielectrophoresis is a promising method for aligning NWs to metal electrodes [6–8], a conceptually simpler method is to directly grown NWs where they will be used, for example, forming nanobridges between two opposing electrodes.

Nanobridge device formation is a method of directed integration in which the bottom up forces that determine NW growth are first patterned using top down methods. So far, there have been several reports of nanobridge devices [9–16] using either catalyst [9,13] or inorganic seed layer mediated growth [10–12,14–16]. Although these previous efforts show promise, they also have disadvantages such as requiring a Au catalyst (potential for contamination), or expensive substrates, such as silicon-on-insulator or reactive ion etching, to fabricate the trench.

Recently, the use of carbonized photoresist (C-PR) was reported as a nucleation layer for producing selective growth of high quality ZnO nanowires from evaporated ZnO powder [17,18]. The C-PR

was reported to have a resistivity similar to ITO [17,19], a frequently used wide band gap conductor, suggesting that C-PR could serve as a built-in electrode for contact to NW devices.

In this work, we demonstrate (1) that the C-PR method can be used as a novel method to form ZnO nanobridge structures, (2) that C-PR can provide Schottky like electrical contact to these nanobridge devices, and (3) operation of these nanobridges as three terminal field effect devices with bottom gate modulation of the conductivity of the *n*-type ZnO channel. The novel use of C-PR is demonstrated to allow simultaneous growth and electrical integration of ZnO nanowires to pre-existing lithographic features without the use of a metal catalyst or inorganic seed layer.

2. Experimental details

Fabrication of nanobridge devices using C-PR (schematically illustrated in Fig. 1) was performed using four main steps, photoresist (PR) deposition and patterning, carbonization, Mo deposition and patterning, and then NW growth. First, 2.5–2.7 μm of MicroChem S1818 PR was coated on SiO₂ covered Si wafers and then patterned into nanobridge nucleation/contact pads using conventional contact lithography. The width of the opposing contact pads varied from 25 to 100 μm and the separation between them varied from 2 to 10 μm.

In the second step, the PR is carbonized. Following the work of Park et al. [19], the PR was carbonized at 900 °C and 5 torr in a reducing atmosphere (95% N₂, 5% H₂). The low pressure and reducing atmosphere are used to minimize the amount of residual oxygen in the tube furnace. The furnace was heated at a ramp rate of 10 °C per minute until 300 °C is reached, where it is held for 30 min to hard bake the PR. The furnace is then heated to 900 °C with a

* Corresponding author.

E-mail addresses: pelatt@eecs.oregonstate.edu (B.D. Pelatt), jconley@eecs.orst.edu (J.F. Conley Jr.).

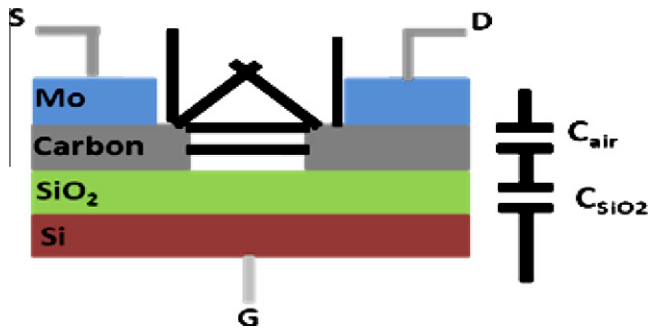


Fig. 1. Schematic of three terminal nanobridge configuration, with modeled gate capacitance.

ramp rate of 10 °C per minute for 1 h to carbonize the photoresist, after which it is allowed to cool to room temperature.

In the third step, a layer of molybdenum (Mo) was then deposited using electron beam evaporation and patterned onto the large pad area using a liftoff technique. Liftoff was achieved using another layer of PR that was patterned and developed to provide windows to the C-PR for Mo deposition. The Mo layer serves as the contact metal pad to the C-PR and prevents nanowire nucleation.

The final step is NW growth. ZnO NWs were grown on the exposed C-PR using the vapor–solid growth method. A metal catalyst was not used. Zn vapor was supplied via carbothermal reduction of ZnO, well described in [20]. Pure ZnO (99.99%, Sigma–Aldrich) and carbon powders (99.9995%, Alpha Aeser) were ground together in a 1:1 ratio and inserted into a tube furnace at the high temperature zone, ~920 °C, and allowed to grow for 60 min. A nitrogen carrier gas at 150 sccm carries the ZnO vapor down the tube, approximately 20 cm, to the patterned C-PR samples, which are at a lower temperature, ~770 °C. A low flow rate of oxygen, approximately 1–2 sccm, is introduced near the samples to aid growth. The precursors are not inserted into the high temperature zone until the furnace has reached temperature to avoid any low temperature nanowire growth.

The C-PR thickness was measured with an Alpha Step Surface Profiler. The resistivity of the C-PR film pre and post NW growth and with and without Mo was performed with a Jandel four point probe. NW growth morphology and uniformity (length, diameter, orientation, density, etc.) were characterized using an FEI dual beam field emission scanning electron microscope (FESEM). Electrical measurements of nanobridge devices were performed using an Agilent 4155C Semiconductor Parameter Analyzer.

3. Results and discussion

3.1. Dimensional characterization of the carbonization process

Due to the devolution of gases such as CO₂, H₂O, and O₂, much of the PR volume is lost as it decomposes during the carbonization process [19,21]. This shrinkage occurs primarily normal to the surface and is a function of pressure and ambient. An initial attempt at carbonization in an N₂ ambient at 5 torr resulted in evaporation of much of the PR and a loss of the PR pattern. This was likely due to the presence of oxygen, which reacts with the carbon to form CO₂. In order to reduce residual O₂ in the tube furnace, subsequent carbonization was performed in a 5% H₂/95% N₂ reducing environment (H₂ reduces residual O₂ by reacting with it to form H₂O). Carbonization at 5 torr in 5% H₂/95% N₂, was found to reduce shrinkage to ~80% in the direction normal to the surface and 1–3% lateral to the surface. These dimensional changes are roughly consistent with what has been reported previously [19,21]. The small amount of lateral shrinkage relative to the vertical shrinkage has been attributed to the formation of a SiC adhesion layer at the C-PR/SiO₂ interface [21]. Despite the relatively large amount of vertical shrinkage, the relatively small change in lateral dimensions was found to be suitable for nanobridge device fabrication.

3.2. Electrical characterization of carbonized photoresist

3.2.1. Pre NW growth

The resistivity of the C-PR was found to be sensitive to the carbonization temperature, time, and ambient. Shown in Fig. 2 are plots of resistivity vs. (a) temperature and (b) time for a C-PR film on SiO₂. Carbonization was performed at 5 torr in a 5% H₂/95% N₂ ambient for (a) and at 5 torr in N₂ for (b). Resistivity was calculated from four point probe measurements of sheet resistance using, $\rho = 4.523t \frac{V}{I}$ where t is the thickness and I and V are the applied current and measured voltage, respectively. C-PR thickness for each data point was determined via profilometer. In all cases, the thickness of the C-PR was measured to be between 250 and 350 nm. Resistivity is seen to decrease with temperature and time. Increased temperature and time both lead to lower resistivity because the amount of graphitization of the C-PR increases [21]. Comparing Fig. 2a and b, it is seen that use of a 5% H₂/95% N₂ ambient results in approximately 10x lower resistivity than for an N₂ ambient. The reducing atmosphere was reported to reduce the oxygen to carbon ratio in the C-PR, which further helps to reduce the resistivity of the C-PR [19]. At higher temperatures and longer

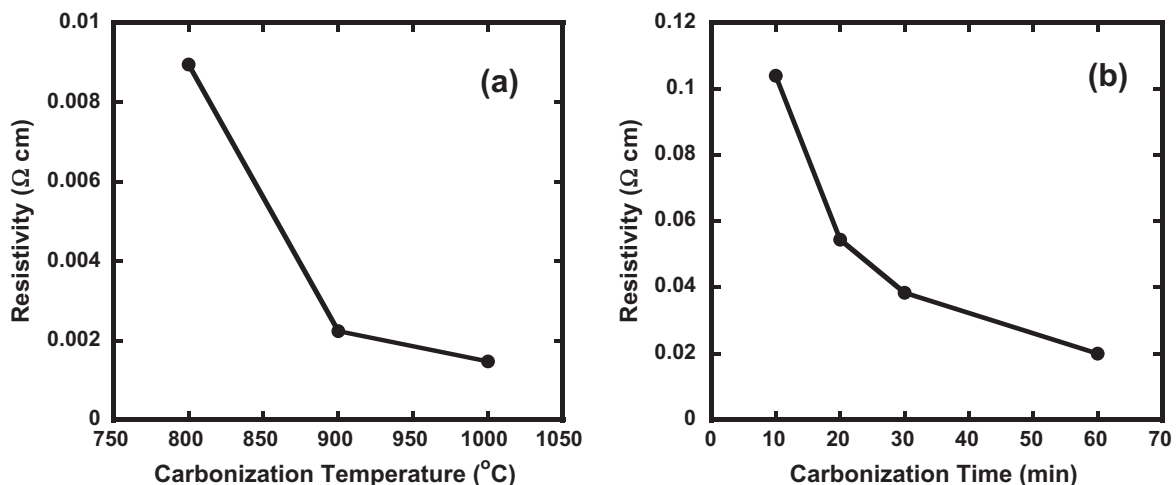


Fig. 2. C-PR pad resistivity vs. (a) carbonization temperature and (b) carbonization time. Ambient in (a) was 5% H₂/95% N₂ ambient in (b) was pure N₂.

times, the reduction in resistivity appears to saturate. Based on Fig. 2, the carbonization conditions chosen for NW growth and device formation were 60 min at 900 °C in a 5% H₂/95% N₂ ambient.

3.2.2. Post NW growth

Cheng et al. [17] reported that prior to any NW growth, as-carbonized C-PR has a resistivity similar to ITO. The resistivity of C-PR following the NW growth process has not been reported previously. Shown in Table 1 is a comparison of C-PR resistivity before and after NW growth, as well as for Mo coated C-PR following NW growth. The NW growth process was found to increase resistivity by approximately an order of magnitude. This increase in resistivity potentially limits the usefulness of the C-PR as a contact material. Thus, to improve the sheet resistance, a capping layer of Mo was used. Mo was chosen because it has a high melting point (2623 °C) and it was found that it does not support growth of ZnO NWs (see Fig. 3). As shown in Table 1, the Mo layer has a sheet resistance three orders of magnitude lower than that of C-PR.

3.3. Nanobridge formation

In this work, C-PR is used as both the nucleation and contact layer, conceptually simplifying the fabrication process. Shown in Fig. 3 is an SEM image of the Mo, C-PR, and SiO₂ surface regions following NW growth. NWs grow predominantly on the C-PR areas with no NW growth observed on the Mo and only very sparse growth on the SiO₂.

The NW growth process on C-PR is thought to be due to the immiscibility of the two materials [22]. The ZnO molecules that land on the C-PR do not adsorb into it, but stay on the surface and agglomerate until larger seed crystals are formed. These then continue to absorb more ZnO until NWs begin to form. The SiO₂ has very low surface energy so the nucleation of ZnO is inhibited [23].

Energy dispersive spectroscopy (EDS) data with corresponding SEM image is illustrated in Fig. 4. The solid yellow line in the SEM image indicates the EDS scan line; the dashed orange lines demarcate different surface regions for the EDS data. The Zn and O signals clearly match the ZnO NW growth area. No Mo was found

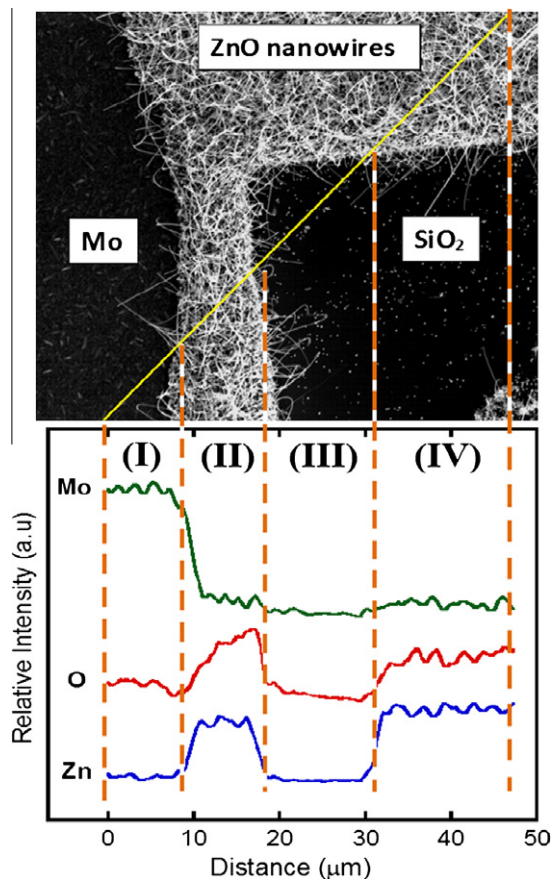


Fig. 4. Energy dispersive spectroscopy (EDS) data with corresponding SEM image.

Table 1

Resistivity comparison for C-PR alone, with, and without Mo.

| Material | Resistivity (Ω-cm) |
|------------------------------|--------------------|
| C-PR | 4×10^{-3} |
| C-PR, post NW growth | 2×10^{-2} |
| C-PR with Mo, post NW growth | 8×10^{-5} |

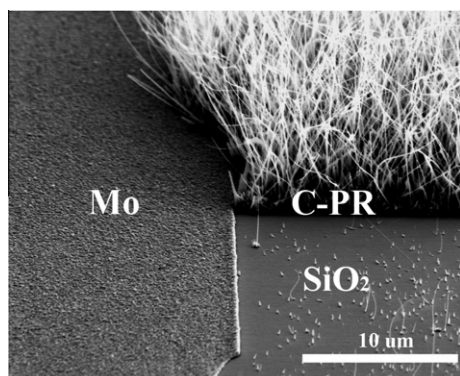


Fig. 3. SEM image of the Mo, SiO₂, and C-PR regions on the surface following NW growth.

in ZnO NWs area (II and IV), showing that Mo does not directly participate in ZnO NW growth. It is worth noting that only a limited amount of Zn appeared on the Mo (I) and SiO₂ (III), suggesting a well defined growth of ZnO nanobridge devices between C-PR pads.

The C-PR method was used to create ZnO nanobridge devices between opposing C-PR pads. Shown in Fig. 5 are top down SEM images of ZnO nanobridges grown (a) with and (b) without Mo pads. A top down image of the complete structure with Mo coated C-PR pads is shown in the inset. While the EDS data in Fig. 4 strongly suggests that Mo is not directly involved in the growth process, the Mo appears to have indirectly changed the morphology of the NWs. A comparison of the images in Fig. 5a and b reveals that for otherwise identical growth conditions ($T \sim 770$ °C, O₂ ~ 150 sccm, N₂ ~ 1 –2 sccm, growth time ~ 30 min), the use of the Mo capping layer resulted in NWs with increased diameter and more ribbon-like in morphology. One possible explanation for this change in morphology is that by preventing NW growth on areas covered by the Mo, the reduction of total surface area available for NW growth made more precursor available for NW growth on uncovered regions.

An angled side view SEM image, shown in Fig. 6, reveals that NW connections between C-PR pads can be made in several ways: (i) single NW direct connections, (ii) fusing of two NWs from two pads, and (iii) possible connection by physical touching of two NWs. Because of the thin layer (300 nm) of C-PR after carbonization, the majority of the NW connections are of types (ii) and (iii) and thus form a three dimensional nanobridge network structure. Current conduction will likely be dominated by type (ii) nanobridge connections.

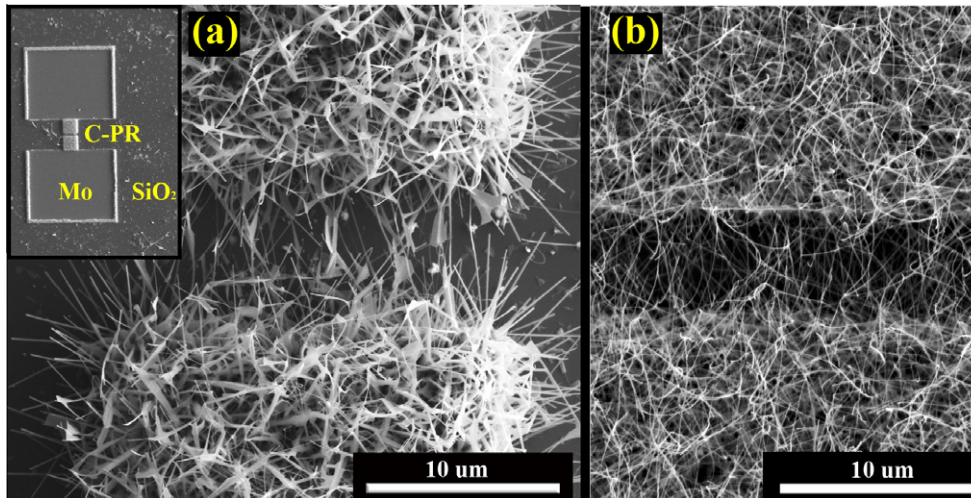


Fig. 5. SEM images of ZnO nanobridges formed (a) with Mo and (b) without Mo coated C-PR pads. Inset shows a top down image of the complete structure.

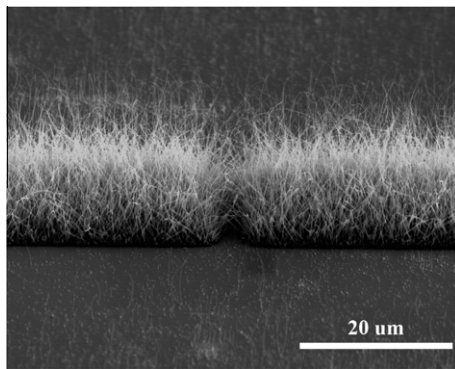


Fig. 6. Side SEM image of ZnO nanobridges.

A series of C-PR pads was fabricated using different pad widths and separations between opposing pads. Tabulated in Table 2 is the estimated average total number of nanobridges for 25, 50, and 100 μm wide pads separated by 5 μm . Tabulated in Table 3 is the estimated average number of nanobridges for a 10 μm section of the center of 50 μm wide pads separated by 2, 3, 5, and 10 μm . The average number of nanobridges is estimated from top down

Table 2

Estimated average number of nanobridges form for different C-PR pad widths. The C-PR separation is 5 μm .

| C-PR pad width (μm) | Total nanobridges |
|----------------------------------|-------------------|
| 100 | 195 \pm 6 |
| 50 | 95 \pm 4 |
| 25 | 45 \pm 4 |

Table 3

Estimated average number of nanobridges formed for different C-PR separations. The C-PR pad width is 50 μm .

| C-PR pad separation (μm) | Nanobridges per 10 μm length |
|---------------------------------------|---|
| 10 | 14 \pm 3 |
| 5 | 45 \pm 3 |
| 3 | 59 \pm 2 |
| 2 | 67 \pm 4 |

SEM images. As expected, an increase in pad separation resulted in a decrease in the average number of nanobridges formed. An increase in C-PR pad width resulted in an increase in the total nanobridge formation, as well as a slight increase in the number of bridges formed per μm . A likely explanation for the slight decrease in the number of bridges per μm in the narrow pads is the rounding of the C-PR pads during the carbonization process – less bridges form near the corners of the pads.

3.4. Electrical characterization

The primary reason for the use of Mo was to reduce the resistance of the ZnO nanobridge structures. The resistance of the C-PR/ZnO nanobridge/C-PR structure was measured to be $1.5 \times 10^6 \Omega$ while the resistance using Mo capping (Mo/C-PR/ZnO nanobridge/C-PR/Mo) was typically in the range of $7.3 \times 10^4 \Omega$. This reduction in resistance led to an increase in the current response of the structures. The maximum current measured when Mo was used was $\sim 20\times$ larger than when Mo was not used.

Mo has good thermal stability, low thermal expansion and high density which can protect the C-PR from oxidization during high temperature growth processing and reduce mechanical damage due to probe contact during electrical measurement. An added benefit of Mo was that it is a much more robust contact layer than C-PR and allowed for greater repeatability of measurements. Although NWs have been used in selectively grown nanobridge configuration previously [9–16]; this is the first time that C-PR has been used as both the nucleation and contact layer.

The nanobridge structures can be operated as a three terminal field effect device with source (S), drain (D), and bottom gate (G) terminals configured as shown in Fig. 1. Shown in Fig. 7 is a plot of Mo/C-PR/ZnO NW/C-PR/Mo pad to pad current (I_d) vs. pad to pad voltage (V_{ds}), for positive, zero, and negative voltage applied to the Si substrate back gate (V_{gs}). As a control experiment, no current was measured between C-PR pads without NW growth.

As seen in Fig. 1, I_d can be modulated by V_g . ZnO is intrinsically an *n*-type semiconductor [24]. A positive gate bias leads to an accumulation of carriers in the NW because the conduction band of the *n*-type semiconductor is expected to be pulled towards the Fermi level, giving an increased density of states near the Fermi level. This accumulation of carriers enhances conductance, increasing I_d . Alternately, a negative gate bias decreases the conductance of the nanobridge because the conduction band is raised upward [25,26]. It can also be seen that the V_{ds} at which the device begins

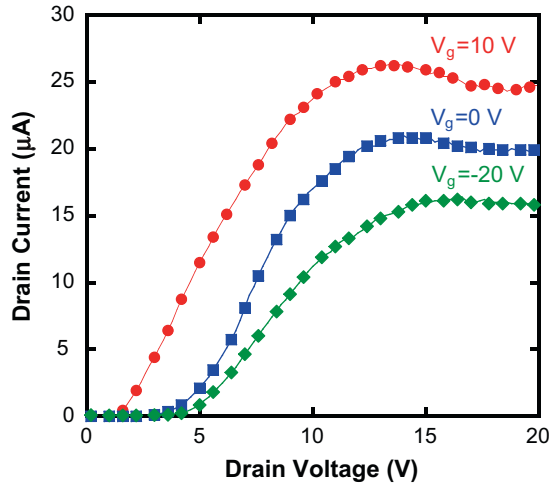


Fig. 7. Plot of I_d - V_{ds} at different gate voltage (V_{gs}) with 25 μm C-PR pad width and 10 μm pad separation.

to conduct strongly shifts negative under positive gate bias and shifts positive for negative gate bias.

Although I_d can be modulated by V_g , the effect is not strong. For example, the nanobridge devices could not be completely turned off by an applied negative V_g . One reason for the weak gate modulation is the small effective gate capacitance of the nanobridge device structure. The gate capacitance is modeled in Fig. 1, schematically showing a contribution from both the SiO_2 and the air gap between the SiO_2 and the nanobridges. As concluded from the SEM image in Fig. 6, the majority of nanobridge are of type (ii), consisting of two fused NWs grown at an angle from the C-PR pads and lying a range of distances from the plane of the C-PR surface. The capacitance for these above plane nanobridges will be very small because air has a low dielectric constant ($\epsilon_{\text{air}} \approx 1$) and will be a function of the distance the nanobridge lies from the surface. Thus, the above plane nanobridges would not feel the effects of an applied gate voltage as strongly as those closest to the bottom gate, leading to reduced current modulation. Another reason that the devices could not be completely turned off was that it was found that physical breakdown of the bottom gate oxide layer occurs before the negative V_g can be reached that would be required to completely turn-off the devices.

Shown in Fig. 8 is a plot of C-PR I_d vs. V_{gs} , for V_{ds} ranging from 0.2 to 0.8 V. The subthreshold slope (SS) of the I_d - V_{gs} curves is quite large, in the range of 9–15 V/decade. As illustrated in Fig. 1 and shown in Fig. 6, there is a wide variation in air gap between the nanobridges and substrate. As previously mentioned, the total gate capacitance can be modeled as a series combination of a fixed SiO_2 capacitance, C_{SiO_2} , and a variable capacitance due to the variable air gap, C_{air} . Because of the variable capacitance, nanowire devices will be turned on over a range of V_{gs} , thus resulting in a large SS.

The turn on voltage (V_{on}) can be roughly estimated by extrapolating the approximately linear region of the I_d vs. V_{gs} curves in the range of 0–10 V back to the x -axis. The carrier concentration, n_e , can be roughly estimated using V_{on} and the electron mobility, μ , can be roughly estimated using the slope of the linear portion. Following the method used in Goldberger et al. [27] for comparison, the carrier concentration is roughly estimated using

$$n_e = \frac{V_{\text{on}} C_g}{q \pi r^2 n L} \quad (1)$$

where q is the charge of the electron, r is the radius of the nanobridges, n is the average number of nanobridges formed between C-PR pads, and L is the length of the nanobridge channel. Multiply-

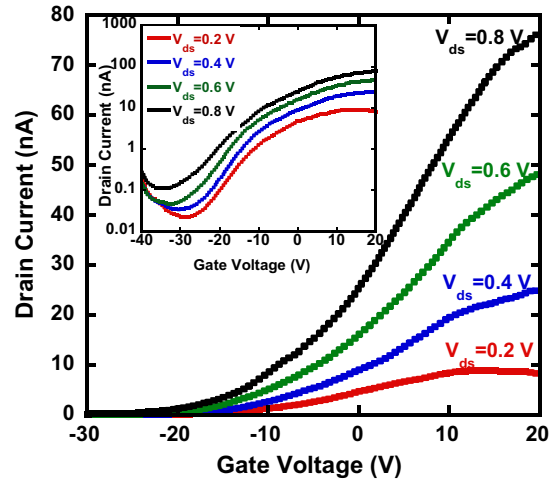


Fig. 8. Drain current (I_d) vs. gate voltages (V_{gs}) measured at drain-source voltage (V_{ds}) from 0.2 to 0.8 V. The inset plot is logarithmic scale of I_d .

ing the average cross sectional area of the nanobridges by the average number of nanobridges formed approximates the total current carrying area of the nanobridge structure. The capacitance is modeled as a cylinder on a plane [27] using

$$C_g = \frac{2\pi\epsilon\epsilon_0 L}{\ln(2h/r)} \quad (2)$$

where ϵ is the effective dielectric constant of the insulator (combination of SiO_2 and air), h the total dielectric thickness and r is the cumulative NW radius calculated from the estimate of the total NW cross sectional area. The mobility can be roughly estimated by

$$\mu = \frac{g_m L^2}{C_g V_{ds}} \quad (3)$$

where g_m is the measured transconductance of the linear portion of the I_d - V_{gs} curve, $g_m = \frac{dI_d}{dV_{gs}}$, C_g is a series combination of the capacitance of the SiO_2 and air between the nanobridges and Si back gate, and L is the average length of the nanobridges.

The mobility thus roughly estimated from Eq. (3) was 40 ± 10 ($\frac{\text{cm}^2}{\text{Vs}}$), the carrier concentration was roughly estimated from Eq. (1) to be $3 \times 10^{18} \pm 6 \times 10^{17}$ (cm^{-3}), and the transconductance was 10 ± 4 nS. (Note that the uncertainty in these estimates is large and is a direct result of the large uncertainty in estimating the number of nanobridges, the relative number of each type of nanobridge connection, the length of the nanobridges, and the height of the air gap between the bottom gate dielectric and nanobridges.) The $I_{\text{on}}/I_{\text{off}}$ ratio is roughly 10^3 . The value of $I_{\text{on}}/I_{\text{off}}$ is small compared to other work, and is a result of the nanobridges being formed at different heights above the substrate. As the gate voltage is increased, some nanowires will conduct when others are still turned off. These estimated values are comparable to other reported nanowire transistor parameters [25,28–31], as shown in Table 4.

Finally, as electrical characterization of the C-PR/ZnO NW system was not performed in previous reports [17,18], it is important to characterize the nature of the electrical contact between the C-PR and ZnO nanobridges. From the I_d - V_{ds} curve shown in Fig. 8, the contact appears to be Schottky type because of the small current at low voltages and the inverse curvature of the I - V curves [32,33]. Following [33] the Mo/C-PR/ZnO nanowire/C-PR/Mo system can be modeled as a metal/semiconductor/metal (MSM) device with the C-PR as the metal and ZnO the semiconductor.

Table 4
Electrical parameter comparison for different groups.

| Group | Mobility ($\frac{\text{cm}^2}{\text{Vs}}$) | Transconductance | Carrier concentration (cm^{-3}) | Current on/off ratio |
|----------------------------|---|------------------|---|----------------------|
| This work | 40 ± 11 | 10 ± 4 nS | $3 \times 10^{18} \pm 6 \times 10^{17}$ | 10^3 |
| Umar [25] | 3.8 | 4 nS | 6.7×10^{13} | 10^3 |
| Liu [28] | 21 | 16 nS | 6×10^{17} | 10^6 |
| Suh (Single NW FET) [29] | 24 | 70 nS | 6×10^{18} | 10^8 |
| Suh (Multiple NW FET) [29] | 30 | 3 μS | 9×10^{17} | 10^2 |
| Verma [30] | 28 | 160 nS | Not reported | 10^6 |
| Subannajui [31] | 928 | 3.06 μS | 8×10^{18} | 10^6 |

The Schottky barrier height for the C-PR/nanowire interface, ϕ_b , can be calculated by [34]

$$\phi_b = \frac{kT}{q} \ln \left(\frac{AAT^2}{I_{ds}} \right) \quad (4)$$

where k is Boltzmann's constant, T the temperature in Celsius, q the charge of the electron, A the contact area, A^* Richardson's constant, and I_s the saturation current. The saturation current is found by extrapolating a semi-log plot of the I_d vs. V_{ds} data from Fig. 7 to $V=0$. The average calculated barrier height, ϕ_b , was found to be approximately 0.35 eV. The barrier height was also calculated for samples without the Mo capping layer. The calculations showed that the barrier without the Mo capping layer had roughly the same value.

Although a disadvantage of Schottky contacts is a high series resistance, which limits the total current in the nanowires at low voltages, Zhou et al. [35] have shown that Schottky contacts can be advantageous for sensing experiments.

4. Conclusion

A new method was presented for the directed growth and integration of ZnO nanobridge devices using carbonized photoresist. The use of PR allows for simple lithographic patterning of the force that directs NW growth and avoids both metal catalysts and inorganic seed layers. Electrical connection to the nanowires occurs simultaneously with nanowire growth. Because C-PR is used for both nucleation and electrical contact, this method allows for simultaneous alignment, growth, and electrical connection of nanowires to lithographic features. Electrical characterization of the C-PR before and after NW growth revealed an increase in sheet resistance. A layer of Mo was incorporated to provide a lower sheet resistance contact to the C-PR layer and to prevent NW growth so as to provide contact pads free of NW growth. EDS data showed that the nanowire growth was highly specific to the C-PR. I - V measurements on the Mo/C-PR/nanobridge device structure confirmed electrical connection between C-PR pads. Three terminal measurements demonstrated field effect modulation of ZnO nanobridge conductivity using the Si substrate as a back gate. The 3D nature of the nanobridges formed between the C-PR terminals may be an advantage for sensing as this allows for more nanobridges per surface area than planar bridges. Overall, these results show that the novel use of C-PR to directly align ZnO NWs to lithographically defined electrodes shows promise for the fabrication and integration of NW transistors and sensors [36].

Acknowledgements

The authors are grateful to the Army Research Laboratory (W911NF-07-2-0083), the Office of Naval Research (N00014-07-1-0457), and Oregon Nanosciences and Microtechnologies Institute (ONAMI) for support, K. McAuliffe for data collection (supported by a National Science Foundation REU supplemental grant 0805372), and C. Tasker for equipment and technical assistance.

References

- Agarwal R, Lieber CM. Semiconductor nanowires: optics and optoelectronics. *Appl Phys A-Mater Sci Process* 2006;85:209–15.
- Cui Y, Wei QQ, Park HK, Lieber CM. Nanowire nanosensors for highly sensitive and selective detection of biological and chemical species. *Science* 2001;293:1289–92.
- Heo YW, Norton DP, Tien LC, Kwon Y, Kang BS, Ren F, et al. ZnO nanowire growth and devices. *Mater Sci Eng R-Rep* 2004;47:1–47.
- Wang ZL. Zinc oxide nanostructures: growth, properties and applications. *J Phys-Condens Matter* 2004;16:R829–58.
- Wang ZL, Song JH. Piezoelectric nanogenerators based on zinc oxide nanowire arrays. *Science* 2006;312:242–6.
- Lao CS, Liu J, Gao PX, Zhang LY, Davidovic D, Tummala R, et al. ZnO nanobelt/nanowire Schottky diodes formed by dielectrophoresis alignment across Au electrodes. *Nano Lett* 2006;6:263–6.
- Fan DL, Zhu FQ, Cammarata RC, Chien CL. Efficiency of assembling of nanowires in suspension by ac electric fields. *Appl Phys Lett* 2006;89:223115.
- Liu YL, Chung JH, Liu WK, Ruoff RS. Dielectrophoretic assembly of nanowires. *J Phys Chem B* 2006;110:14098–106.
- Lee JS, Islam MS, Kim S. Direct formation of catalyst-free ZnO nanobridge devices on an etched Si substrate using a thermal evaporation method. *Nano Lett* 2006;6:1487–90.
- Conley JF, Stecker L, Ono Y. Directed integration of ZnO nanobridge devices on a Si substrate. *Appl Phys Lett* 2005;87.
- Li YB, Della Valle F, Simonnet M, Yamada I, Delaunay JJ. High-performance UV detector made of ultra-long ZnO bridging nanowires. *Nanotechnology* 2009;20:045501.
- Ahn MW, Park KS, Heo JH, Kim DW, Choi KJ, Park JG. On-chip fabrication of ZnO-nanowire gas sensor with high gas sensitivity. *Sens Actuator B-Chem* 2009;138:168–73.
- Islam MS, Sharma S, Kamins TI, Williams RS. Ultrahigh-density silicon nanobridges formed between two vertical silicon surfaces. *Nanotechnology* 2004;15:L5–8.
- Conley Jr JF, Stecker L, Ono Y. Directed assembly of ZnO nanowires on a Si substrate without a metal catalyst using a patterned ZnO seed layer. *Nanotechnology* 2005;16:292–6.
- Conley Jr JF, Stecker L, Ono Y. Selective growth and directed integration of ZnO nanobridge devices on si substrates without a metal catalyst using a ZnO seed layer. *J Electron Mater* 2006;35:795–802.
- Gao P-X, Liu J, Buchine BA, Weintraub B, Wang ZL, Lee JL. Bridged ZnO nanowires across etched electrodes. *Appl Phys Lett* 2007;91:142108.
- Cheng C, Lei M, Feng L, Wong TL, Ho KM, Fung KK, et al. High-quality ZnO nanowire arrays directly fabricated from photoresists. *ACS Nano* 2009;3:53–8.
- Li PG, Tang WH, Wang X. Synthesis of ZnO nanowire arrays and their photoluminescence property. *J Alloy Compd* 2009;479:634–7.
- Park BY, Taherabadi L, Wang CL, Zoval J, Madou MJ. Electrical properties and shrinkage of carbonized photoresist films and the implications for carbon microelectromechanical systems devices in conductive media. *J Electrochem Soc* 2005;152:J136–43.
- Huang MH, Wu YY, Feick H, Tran N, Weber E, Yang PD. Catalytic growth of zinc oxide nanowires by vapor transport. *Adv Mater* 2001;13:113–6.
- Du RB, Ssenyange S, Aktary M, McDermott MT. Fabrication and characterization of graphitic carbon nanostructures with controllable size, shape, and position. *Small* 2009;5:1162–8.
- Yang YH, Wang B, Yang GW. Mechanisms of self-catalyst growth of agave-like zinc oxide nanostructures on amorphous carbons. *Cryst Growth Des* 2007;7:1242–5.
- Chung TF, Luo LB, He ZB, Leung YH, Shafiq I, Yao ZQ, et al. Selective growth of catalyst-free ZnO nanowire arrays on Al: ZnO for device application. *Appl Phys Lett* 2007;91:233112.
- Ozgur U, Alivov YI, Liu C, Teke A, Reshchikov MA, Dogan S, et al. A comprehensive review of ZnO materials and devices. *J Appl Phys* 2005;98:041301.
- Umar A, Park YK, Hahn YB. High aspect-ratio ZnO nanowires based nanoscale field effect transistors. *J Nanosci Nanotech* 2009;9:2693–7.
- Fan Z, Lu JG. Electrical properties of ZnO nanowire field effect transistors characterized with scanning probes. *Appl Phys Lett* 2005;86:032111.
- Goldberger J, Sirbully DJ, Law M, Yang P. ZnO nanowire transistors. *J Phys Chem B* 2005;109:9–14.
- Liu Y, Zhang Z, Xu H, Zhang L, Wang Z, Li W, et al. Visible light response of unintentionally doped ZnO nanowire field effect transistors. *J Phys Chem C* 2009;113:16796–801.

- [29] Suh D-I, Lee S-Y, Hyung J-H, Kim T-H, Lee S-K. Multiple ZnO nanowires field-effect transistors. *J Phys Chem B* 2008;112:1276–81.
- [30] Verma VP, Jeon H, Hwang S, Jeon M, Choi W. Enhanced electrical conductance of zno nanowire FET by nondestructive surface cleaning. *IEEE Trans Nanotech* 2008;7:782–6.
- [31] Subannajui K, Kim DS, Zacharias M. Electrical analysis of individual ZnO nanowires. *J Appl Phys* 2008;104:014308.
- [32] Lepselter MP, Sze SM. An insulated gate field effect transistor using Schottky barrier contacts for source and drain. *Proc IEEE* 1968:1400.
- [33] Sze S, Ng K. *Physics of semiconductor devices*. 3rd ed. Wiley-Interscience; 2006.
- [34] Schroder DK. *Semiconductor material and device characterization*. 3rd ed. Wiley-Interscience; 2006. p. 158.
- [35] Zhou J, Gu Y, Hu Y, Mai W, Yeh PH, Bao G, et al. Gigantic enhancement in response and reset time of ZnO UV nanosensor by utilizing Schottky contact and surface functionalization. *Appl Phys Lett* 2009;94:11031–3.
- [36] Huang CC, Pelatt BD, Conley Jr JF. Directed integration of ZnO nanobridge sensors using photolithographically patterned carbonized photoresist. *Nanotechnology* 2010;21:195307.